Bioactive Materials 14 (2022) 321–334

Contents lists available at ScienceDirect

Bioactive Materials

journal homepage: www.keaipublishing.com/en/journals/bioactive-materials

In-biofilm generation of nitric oxide using a magnetically-targetable cascade-reaction container for eradication of infectious biofilms

Guang Yang [a,b], Da-Yuan Wang [a,b], Yong Liu [a], Fan Huang [d], Shuang Tian [a,b], Yijin Ren [c], Jianfeng Liu [d,**], Yingli An [a], Henny C. van der Mei [b,***], Henk J. Busscher [a,b,****], Linqi Shi [a,*]

[a] State Key Laboratory of Medicinal Chemical Biology, Key Laboratory of Functional Polymer Materials, Ministry of Education, Institute of Polymer Chemistry, College of Chemistry, Nankai University, Tianjin, 300071, PR China
[b] University of Groningen and University Medical Center Groningen, Department of Biomedical Engineering, Antonius Deusinglaan 1, 9713, AV, Groningen, the Netherlands
[c] University of Groningen and University Medical Center Groningen, Department of Orthodontics, Hanzeplein 1, 9700, RB, Groningen, the Netherlands
[d] Key Laboratory of Radiopharmacokinetics for Innovative Drugs, Chinese Academy of Medical Sciences, and Institute of Radiation Medicine, Chinese Academy of Medical Sciences & Peking Union Medical College, Tianjin, 300192, PR China

ARTICLE INFO

Keywords:
Magnetic nanoparticles
Bacterial infection
Glucose
Reactive-oxygen-species
Intra-vital window

ABSTRACT

Cascade-reaction chemistry can generate reactive-oxygen-species that can be used for the eradication of infectious biofilms. However, suitable and sufficient oxygen sources are not always available near an infection site, while the reactive-oxygen-species generated are short-lived. Therefore, we developed a magnetic cascade-reaction container composed of mesoporous Fe_3O_4@SiO_2 nanoparticles containing glucose-oxidase and L-arginine for generation of reactive-oxygen-species. Glucose-oxidase was conjugated with APTES facilitating coupling to Fe_3O_4@SiO_2 nanoparticles and generation of H_2O_2 from glucose. L-arginine was loaded into the nanoparticles to generate NO from the H_2O_2 generated. Using an externally-applied magnetic field, cascade-reaction containers could be homogeneously distributed across the depth of an infectious biofilm. Cascade-reaction containers with coupled glucose-oxidase were effective in killing planktonic, Gram-positive and Gram-negative bacteria. Additional efficacy of the L-arginine based second cascade-reaction was only observed when H_2O_2 as well as NO were generated in-biofilm. *In vivo* accumulation of cascade-reaction containers inside abdominal *Staphylococcus aureus* biofilms upon magnetic targeting was observed real-time in living mice through an implanted, intra-vital window. Moreover, vancomycin-resistant, abdominal *S. aureus* biofilms could be eradicated consuming solely endogenous glucose, without any glucose addition. Herewith, a new, non-antibiotic-based infection-control strategy has been provided, constituting a welcome addendum to the shrinking clinical armamentarium to control antibiotic-resistant bacterial infections.

1. Introduction

Development of new antibiotics to face the increasing threat of antimicrobial-resistant bacterial infections seems futile [1], considering the ever-shorter time between market-introduction and the appearance of the first signs of bacterial resistance against a new antibiotic [2]. Non-antibiotic-based infection-control strategies are therefore considered preferable [3–5] and more likely to yield return of investment upon market introduction and associated clinical benefits than the development of new antibiotics.

Cascade-reaction chemistry is rapidly emerging as a possible new, bacterial infection-control strategy. In a liner cascade-reaction at least

Peer review under responsibility of KeAi Communications Co., Ltd.
* Corresponding authors.
** Corresponding author.
*** Corresponding author.
**** Corresponding author. State Key Laboratory of Medicinal Chemical Biology, Key Laboratory of Functional Polymer Materials, Ministry of Education, Institute of Polymer Chemistry, College of Chemistry, Nankai University, Tianjin, 300071, PR China.
E-mail addresses: liujianfeng@irm-cams.ac.cn (J. Liu), h.c.van.der.mei@umcg.nl (H.C. van der Mei), h.j.busscher@umcg.nl (H.J. Busscher), shilinqi@nankai.edu.cn (L. Shi).

https://doi.org/10.1016/j.bioactmat.2022.01.044
Received 1 November 2021; Received in revised form 10 January 2022; Accepted 26 January 2022
Available online 10 February 2022

two chemical reactions are integrated, of which each subsequent reaction can only start when the previous reaction step has been completed and the product of the first reaction becomes the substrate for the second reaction [6]. Enzymatic, liner cascade-reactions widely occur in living organisms and are currently considered for use in cancer [7] and infection therapy [8]. Transforming naturally occurring substrates in the human body such as endogenous glucose into oxygen species in a first reaction, a second cascade-reaction can produce antibacterial Reactive Oxygen Species (ROS), including NO. ROS can degrade the Extracellular Polymeric Substance (EPS) matrix of an infectious biofilm [9], disrupt bacterial cell membranes [10] and damage intra-cellular DNA [11]. Bacterial resistance against ROS is relatively infrequent, although some bacterial species are known to have developed resistance against specific types of ROS, such as $\bullet O_2^-$ and H_2O_2, but not against $\bullet OH$, $^1O_2$ [12] and NO [13]. Resistance against $\bullet O_2^-$ and H_2O_2 is generally attributed to the upregulation of genes involved in the synthesis of endogenous antioxidants, that can be enzymatic or non-enzymatic in nature [12].

Enzymatic, liner cascade-reactions for infection-control [3,5,14] can generate different types of ROS at the same time [15], killing both Gram-positive and Gram-negative bacterial strains [3,16]. The main challenge in the application of enzymatic, liner cascade-reactions is to keep the enzymatic initiators and the reaction products together in a suitable reaction container [6]. In addition, for eradication of infectious biofilms, the short life-time of most ROS [17,18] necessitates ROS generation in the close vicinity of the target bacteria. This suggests that at least the second cascade-reaction generating ROS should occur within an infectious biofilm. This constitutes a second challenge in the application of enzymatic, liner cascade-reactions in infection-control. A possible way to force in-biofilm ROS generation, would be to use mesoporous, magnetic nanoparticles as a cascade-reaction container. Magnetic nanoparticles can be driven into a biofilm by application of a suitable, externally applied magnetic field [19–21].

Therefore, we here developed a magnetically targetable cascade-reaction container based on magnetic, mesoporous Fe_3O_4@SiO_2 nanoparticles with coupled glucose-oxidase and loaded with L-arginine. Uniquely, this cascade-reaction system generates NO without the presence of suitable, endogenous oxygen-species, but consuming only glucose (Scheme 1). NO generated through cascade-reaction chemistry has not yet been applied for the control of infectious biofilms (see Tables S1, S2 and S3 for a comprehensive overview of antibacterial applications of cascade-reaction chemistry for planktonic bacteria, bacteria in a biofilm-mode of growth and infection-control *in vivo*, respectively). NO possesses a significantly longer life-time than other types of ROS [18,22], which makes it an ideal ROS to bridge the distance from its generation site to a target bacterium within its life-time. Moreover, NO has a broad-spectrum antibacterial efficacy and no known mechanism of inducing resistance amongst bacterial pathogens [13]. *In vitro* efficacy of these magnetic, mesoporous Fe_3O_4@SiO_2 cascade-reaction containers will be evaluated against vancomycin-resistant Gram-positive (*Staphylococcus aureus*) and Gram-negative (*Escherichia coli)* bacteria in their biofilm-mode of growth. *In vivo* advantages will be demonstrated by real-time observation of the biodistribution and magnetic targeting of the cascade-reaction container into a vancomycin-resistant, abdominal *S. aureus* biofilm grown underneath an intra-vital abdominal imaging window in mice [23]. Biofilm eradication by targeted cascade-reaction containers is compared with the eradication achieved using vancomycin.

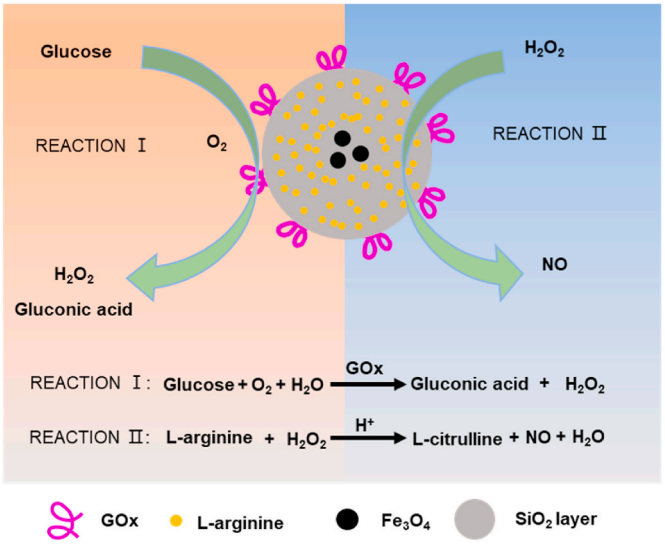

Scheme 1. Magnetic, mesoporous Fe_3O_4@SiO_2 nanoparticles with coupled glucose-oxidase (GOx) and loaded with L-arginine as a cascade-reaction container. The cascade-reaction container can be magnetically targeted to an infectious biofilm for in-biofilm generation of NO to kill infectious bacteria. Cascade-reaction I transforms glucose into gluconic acid and H_2O_2 as assisted by glucose-oxidase, while in cascade-reaction II the H_2O_2 generated oxidizes L-arginine into NO.

2. Experimental

2.1. Materials

Cetyltrimethylammonium chloride (CTAC), tetraethyl orthosilicate (TEOS), 3-aminopropyltriethoxysilane (APTES), triethanolamine (TEOA), ferric chloride ($FeCl_3$), ferrous chloride tetrahydrate ($FeCl_2{\cdot}4H_2O$), ammonium hydroxide (25 wt%, $NH_3{\cdot}H_2O$), L-arginine, 1-(3-dimethylaminopropyl)-3-ethylcarbodiimide hydrochloride (EDCI), Rhodamine B (RhB), N-hydroxysuccinimide (NHS), glucose-oxidase (GOx), were purchased from Sigma-Aldrich. H_2O_2 Assay Kit, NO Assay Kit and Cell Counting Kit-8 (CCK-8) were purchased from Beyotime Biotechnology. All reagents were of analytical grade and used as supplied without further purification. All aqueous solutions were prepared with ultrapure water (resistance >18 MΩ cm^{-1}) from a Milli-Q system.

2.2. Preparation of mesoporous Fe_3O_4@SiO_2 nanoparticles

20 mg of $FeCl_3$ and 20 mg of $FeCl_2{\cdot}4H_2O$ were dissolved in 100 mL of ultrapure water under vigorous stirring in N_2 for 1 h after which 100 μL of concentrated $NH_3{\cdot}H_2O$ was added. After 1 h, 500 mg of CTAC and 500 μL of TEOA were added under stirring. After another 1 h, 3 g of TEOS was dropped into the reaction solution and the reaction was continued for 5 h at 80 °C. The resulting Fe_3O_4@SiO_2 nanoparticles was collected by centrifugation (6445 g, 20 min) and washed three times with ultrapure water. To create mesoporosity, the CTAC template was removed by triple extraction in ethanol (100 mL) containing HCl (1 mL) for 6 h at 70 °C. Mesoporous Fe_3O_4@SiO_2 nanoparticles were collected by centrifugation (6445 g, 20 min), washed in ultrapure water for three times and dried for 6 h at 60 °C to obtain mesoporous Fe_3O_4@SiO_2 nanoparticles.

2.3. Coupling of glucose-oxidase to mesoporous Fe_3O_4@SiO_2 nanoparticles

Glucose-oxidase (GOx) was covalently coupled onto the surface of mesoporous Fe_3O_4@SiO_2 nanoparticles with the aid of APTES. 76 mg of EDCI, 114 mg of NHS and 1 mg glucose-oxidase were dissolved in 5 mL ultrapure water after which 100 μL APTES was added. Glucose-oxidase reacted with APTES through dehydration condensation between amino groups in APTES and carboxyl groups of glucose-oxidase under stirring at 4 °C for 24 h. Amino-functionalized glucose-oxidase (APTES-GOx) obtained was purified in a dialysis bag with molecular weight cut off of 3500 Da against ultrapure water for 36 h and lyophilized for further experiments. Reactions were monitored using ^1H or ^{29}Si NMR

spectroscopy at a 400 MHz (Brüker, Avance III WB 400, Germany). To this end, 8 mg of GOx or APTES-GOx were dissolved in 0.5 mL methyl sulfoxide-d6, while nanoparticles were grinded before suspending the resulting fine powder (50 mg) in the methyl sulfoxide-d6 solution.

2.4. Loading of mesoporous Fe_3O_4@SiO_2 nanoparticles with L-arginine

Mesoporous Fe_3O_4@SiO_2 nanoparticles with coupled glucose-oxidase were loaded with L-arginine by adding L-arginine to a nanoparticle suspension at a glucose-oxidase to L-arginine mass ratio of 1 : 10 in ultrapure water. The suspension was gently stirred for 36 h at room temperature after which mesoporous Fe_3O_4@SiO_2 nanoparticles with coupled glucose-oxidase and loaded with L-arginine were collected through centrifugation (6445 g, 20 min). Nanoparticles were washed three times in ultrapure water and vacuum-dried in an oven for further experiments.

2.5. Characterization of mesoporous, magnetic Fe_3O_4@SiO_2 nanoparticles

Nanoparticles were imaged using Transmission Electron Microscopy (TEM; Talos F200C, FEI, USA) at an acceleration voltage of 200 kV. To this end, samples were prepared by dropping a nanoparticle suspension in ultrapure water onto a carbon-coated copper grid and slow drying in vacuum at room temperature. Magnetization of mesoporous Fe_3O_4@SiO_2 nanoparticles was measured at room temperature using a MPMS-XL-5 superconducting quantum interference device (SQUID) magnetometer (Quantum Design, SQUID VSM, USA) with an intervention magnetic field from −10 kOe to 10 kOe. Elemental surface composition of the nanoparticles was derived from X-ray Photoelectron Spectroscopy (Thermo, Thermo Scientific ESCALAB 250Xi, USA) under Al Kα X-ray radiation (1486.6 eV). Wide-scan photo-electron binding energy spectra were taken at a pass energy of 100 eV and step size of 1 eV, while narrow-scan spectra were obtained at a pass energy of 20 eV and step size of 0.1 eV, setting the C_{1s} binding energy peak at 284.8 eV. Surface area and pore size of the mesoporous nanoparticles were derived from N_2 adsorption-desorption isotherms, recorded on a Micromeritics instrument (ASAP 2460, USA) at 77 K. To this end, mesoporous Fe_3O_4@SiO_2 nanoparticles were first degassed in a vacuum at 150 °C for 6 h, after which N_2 adsorption-desorption isotherms were measured at 77 K. Surface area was calculated using the Brunauer-Emmett-Teller (BET) method. Pore size distribution was obtained from the desorption branch using the Barrett-Joyner-Halenda (BJH) method. For FTIR spectroscopy, nanoparticles, glucose-oxidase and L-arginine were pressed in KBr pellets (1 : 100 by weight). Spectra were collected on an FTS 6000 FTIR spectrometer (Bio-Rad, Hercules, USA) using 128 scans at 8 cm^{-1} resolution. Thermogravimetric (TG) analyses (NETZSCH, TG209, Germany) were conducted over the range from 50 °C to 800 °C under nitrogen flow, applying a heating rate of 10 °C min^{-1}. UV–vis absorption spectra were measured on a UV–vis spectrophotometer (Shimadzu, Tokyo, Japan).

2.6. Measurement of H_2O_2, NO and •OH generation

H_2O_2, NO and •OH generated by mesoporous Fe_3O_4@SiO_2 nanoparticles were quantitated using a Hydrogen Peroxide Assay Kit (Beyotime Biotechnology, Shanghai, China) and Griess reagent (Beyotime Biotechnology, Shanghai, China), respectively. Both assays are based on measuring UV–vis absorbances (UV–vis microplate reader, Spark, TECAN, Austria) and preparation of a standard curve. A standard curve for H_2O_2 was used to relate H_2O_2 concentrations with the UV–vis absorbance at 560 nm (Fig. S1a), while for NO the UV–vis absorbance at 540 nm was employed for preparing a standard curve (Fig. S1b). For the measurement of •OH generation through catalysis of Fe_3O_4, 1 mL of Phosphate Buffered Saline (PBS; 1.8 mM KH_2PO_4, 10 mM Na_2HPO_4, 137 mM NaCl and 2.7 mM KCl, pH 7.4) with suspended Fe_3O_4@SiO_2 nanoparticles (final concentration 800 μg mL^{-1}) was mixed with terephthalic acid (5 mM) and H_2O_2 (10 mM) at pH 5.0 or pH 7.4 at 37 °C in the dark, to yield fluorescent 2-hydroxyterephthalic acid (Fig. S2a). After different time intervals, fluorescence emission between 360 and 550 nm (see Fig. S2b and Fig. S2c for pH 5.0 and 7.4, respectively) was measured upon excitation at 315 nm, after preparation of a standard curve (Fig. S2d and Fig. S2e for pH 5.0 and 7.4, respectively).

2.7. Bacterial culturing and harvesting

Bacterial strains were grown from frozen stock at 37 °C in ambient air. Two Gram-positive (*S. aureus* ATCC12600^{GFP} and *S. aureus* Xen36) and one Gram-negative (*E. coli* Xen14) bacterial strains were cultured on tryptone soy broth (TSB, OXOID, Basingstoke, U.K.) and Luria Bertani agar plates (LB, OXOID, Basingstoke, U.K), respectively. Agar plates were supplemented with 10 μg mL^{-1} tetracycline for *S. aureus* ATCC12600^{GFP}, and with 200 μg mL^{-1} or 30 μg mL^{-1} kanamycin for *S. aureus* Xen36 or *E. coli* Xen14, respectively. For experiments, one colony was transferred from the agar plates into 10 mL liquid medium incubated at 37 °C for 24 h in ambient air. Subsequently, this pre-culture was diluted 1 : 20 in 200 mL of liquid medium and grown for 16 h at 37 °C. Cultures were harvested by centrifugation at 5000*g* for 5 min at 4 °C, washed twice using PBS and sonicated 3 times for 10 s (Vibra cell model 375, Sonics and Material, Inc., Danbury, CT) in an ice/water bath to obtain suspensions with single bacteria. For experiments involving planktonic bacteria, the bacterial concentration in growth medium (TSB or LB) was adjusted to 2×10^6 bacteria mL^{-1}, as enumerated using a Bürker-Türk counting chamber. For initiating bacterial adhesion as the starting point for biofilm growth, bacteria were suspended in PBS to a concentration of 1×10^8 bacteria mL^{-1}, as also enumerated using a Bürker-Türk counting chamber.

2.8. Killing efficacy of planktonic bacteria in vitro

100 μL of a bacterial suspension in TSB or LB (2×10^6 bacteria mL^{-1}) supplemented with 1600 μg mL^{-1} glucose was added into a 96-wells plate after which 100 μL of a nanoparticle suspension or vancomycin solution was added to a final concentration of 80 μg mL^{-1} or 5 μg mL^{-1}, respectively. All strains were resistant to vancomycin (see Table S4 for MIC values). After growth at 37 °C in ambient air for different time intervals up to 6 h, 10 μL aliquots were taken from each suspension serially diluted, and plated on TSB or LB agar plates. After 24 h at 37 °C in ambient air, the number of CFUs was enumerated.

2.9. Magnetic targeting of Rhodamine-B labeled mesoporous Fe_3O_4@SiO_2 nanoparticles in staphylococcal biofilms in vitro

For biofilm formation, 500 μL of *S. aureus* ATCC12600^{GFP} suspension (1×10^8 bacteria mL^{-1}) in PBS was added onto a sterile (5 × 5 mm^2, L × W) poly (methyl methacrylate) plate, placed in a confocal dish (14 mm diameter) to allow bacterial adhesion at 37 °C in ambient air for 1 h. Then, the plate was washed with PBS to remove non-adhering bacteria and 1 mL of TSB was added to grow the adhering staphylococci into a biofilm. After 48 h at 37 °C in ambient air, plates with adhering biofilms were gently washed with PBS.

In order to visualize depth-dependent distribution of mesoporous Fe_3O_4@SiO_2 nanoparticles after magnetic targeting in staphylococcal biofilms, mesoporous Fe_3O_4@SiO_2 nanoparticles were first labeled with red-fluorescent Rhodamine-B. To this end, red-fluorescent Rhodamine-B was coupled to mesoporous Fe_3O_4@SiO_2 nanoparticles after reacting with APTES to obtain amino-functionalized Rhodamine-B that could be directly coupled to Fe_3O_4@SiO_2 nanoparticles, similarly as described for glucose-oxidase coupling (see Fig. S3 for UV–vis and fluorescence emission spectra of mesoporous Fe_3O_4@SiO_2 nanoparticles labeled with Rhodamine-B). Next, green-fluorescent *S. aureus* ATCC126000^{GFP} biofilms were exposed to red-fluorescent mesoporous Fe_3O_4@SiO_2

nanoparticles with coupled glucose-oxidase and loaded with L-arginine suspension (100 μg mL^{-1}) at 37 °C with or without magnetic field exposure up to 60 min. The magnetic field was created employing a cylindrical NdFeB magnet (2 mm thickness and 16 mm in diameter) with 1.26–1.29 T residual magnetism. Subsequently, the nanoparticle suspension was removed, the biofilm was gently washed and imaged using Confocal Laser Scanning Microscopy (CLSM; TCS SP8, Leica, Wetzlar, Germany). GFP and Rhodamine-B were excited employing an argon ion laser at 488 nm and 560 nm, respectively, while fluorescence was collected using Perkin Elmer (London, UK) spectrometer between 500 and 535 nm for GFP and between 580 and 680 nm for Rhodamine-B. Leica software, version 2.0 and Image J software were used to analyze the images obtained.

2.10. In vitro killing efficacy of bacteria in their biofilm-mode of growth

In order to access killing efficacy of mesoporous Fe_3O_4@SiO_2 nanoparticles with coupled glucose-oxidase and loaded with L-arginine against bacteria in their biofilm-mode of growth, 48 h-old bacterial biofilms grown as described above (section 2.9), were exposed to 100 μL of a suspension mesoporous Fe_3O_4@SiO_2 nanoparticles (300 μg mL^{-1}) or a vancomycin solution (10 μg mL^{-1}), respectively. After exposure to a magnetic field, biofilms were further grown up to 6 h, after which biofilms were scraped off and re-suspended in PBS by sonication. 10 μL aliquots were taken from the bacterial suspensions, serially diluted, and plated on a TSB or LB agar plate. After 24 h growth at 37 °C in ambient air, the CFUs were enumerated on each plate.

2.11. In vitro cytotoxicity

NIH/3T3 mouse embryonic fibroblasts were employed to examine cytotoxicity of Fe_3O_4@SiO_2 nanoparticles with coupled GOx and loaded with L-arginine. Fibroblasts were grown in DMEM culture medium supplemented with 10% fetal bovine serum and 1% penicillin-streptomycin at 37 °C in a humidified incubator with 5% CO_2. First, cells were seeded in a 96-wells plate at a density of around 10^4 cells per well for 24 h. After 24 h, cells were gently washed with PBS for three times, and exposed for another 24 h to cascade-reaction containers suspended in DMEM at different concentrations up to 1200 μg mL^{-1}. Viability of the fibroblast layer was assessed using a Cell Counting Kit-8 (CCK-8) assay. To this end, a 10 v/v% CCK-8 solution in DMEM added to each well and incubated for another 1.5 h. Finally, cell viability was evaluated by measuring the absorbance at 450 nm of each well using a microplate reader (SpectraMax M2, MDC, USA). Absorbance measured after cell growth in absence of cascade-reaction containers was set at 100%.

2.12. In vivo eradication of an infectious staphylococcal biofilm underneath an abdominal intra-vital window in mice

7-8 week-old BALB/c nude mice were obtained from Vital River Laboratory Animal Technology Co. (Beijing, China). All animals experiment procedures were approved by the Institutional Animal Care and Use Committee of Nankai University, Tianjin, China. For experiments, mice were equipped with an abdominal intra-vital window [23] made of a custom-made titanium ring (12 mm diameter), equipped with a glass coverslip. For biofilm growth, 200 μL of *S. aureus* ATCC12600^{GFP} suspended in PBS (1×10^9 bacteria mL^{-1}) was injected underneath the abdominal intra-vital window and allowed to grow for 48 h.

In order to study magnetic targeting *in vivo*, first, 200 μL of PBS with Rhodamine-B labeled mesoporous Fe_3O_4@SiO_2 nanoparticles (800 μg mL^{-1}) with coupled glucose-oxidase and loaded with L-arginine suspension was intravenously injected in the tail-vein of 24 mice and targeted to the abdominal infection site by fixing a magnet against the window using medical tape. In one group of 12 mice, no magnetic targeting was applied, while in a second group of 12 mice magnetic targeting was applied. Magnetic targeting was done without anesthesia (for scheme, see Fig. 8a). For bio-optical imaging, mice were anesthetized by intraperitoneal injection of 0.3 wt% pentobarbital sodium (40 mg kg^{-1}) at each selected time point and red fluorescence distribution across the entire body of the mice was imaged using the IVIS Lumina II Imaging System (Perkin Elmer, image acquisition factors: 0.5 s exposure time, emission wavelength 600 nm, excitation wavelength 530 nm medium binning, 1 F/Stop, Open Emission Filter). Images were automatically corrected for background noise and were analyzed through Living Image software (PerkinElmer). Biodistribution of the mesoporous Fe_3O_4@SiO_2 nanoparticles with coupled glucose-oxidase and loaded with L-arginine over different organs was subsequently studied by sacrificing three mice in each group at different points in time, i.e. 1 h, 6 h, 12 h and 24 h after injection, according to the scheme presented in Fig. 8a. Note, that magnetic-targeting was initiated immediately upon injection for 4 h, implying magnetic-targeting was still in process at 1 h. After sacrifice at different time points, abdominal, intra-vital windows were removed and tissue of primary organs (heart, liver, spleen, lungs, kidneys) and tissue surrounding the window was excised and weighted. Then, the different tissues were homogenized in 500 μL PBS and centrifuged at 10,000 g for 10 min. Supernatants were dispersed in 4 mL plasma and red-fluorescence intensity determined as a measure of accumulation of cascade-reaction containers in the tissues through fluorescence spectrophotometer (Perkin Elmer, London, UK). Fluorescence intensities are expressed as a percentage of the fluorescence of the total injected dose and has been normalized with respect to the weight of the organs or excised tissue surrounding the window.

In a separate series of experiments aimed at longer term evaluation of treatment (for scheme, see Figs. 8d), 48 h-old biofilms were grown as described above in mice and infected mice were divided into four groups that were tail-vein injected every other day starting at day 0 up to day 4 with: (1) PBS, (2) 200 μL vancomycin in PBS (500 μg mL^{-1}), (3) 200 μL mesoporous Fe_3O_4@SiO_2 nanoparticles with coupled glucose-oxidase and loaded with L-arginine suspensions in PBS (800 μg mL^{-1}) without magnetic field exposure, (4) 200 μL mesoporous Fe_3O_4@SiO_2 nanoparticles with coupled glucose-oxidase and loaded with L-arginine suspensions in PBS with magnet field exposure. The latter group (4) actually comprised three sub-groups, that were injected with different concentrations of nanoparticles (400, 800 or 1200 μg mL^{-1}). Each of the six (sub-)groups was comprised of three mice. Experiments with different concentration of nanoparticles were done first in order to determine the optimal concentration for *in vivo* eradication of infection in mice. Magnetic field exposure started immediately after injection and was done for 4 h. Magnetic field exposure was repeated every other day up to 4 days, immediately after injection. Biofilms underneath the abdominal, intra-vital windows were imaged every other day till sacrifice. To this end, anesthetized mice were placed on a custom-designed stage of a two-photon laser scanning confocal microscope (Olympus Corporation, Tokyo, Japan; FV1200 MPE), with the window-frame fixed in a clamp to ensure proper focusing. For imaging, an excitation wavelength of 830 nm was employed to visualize green-fluorescent bacteria (emission wavelength 500–535 nm). Bacterial biomass was derived from the number of green-fluorescent voxels and expressed relative to the number of green fluorescence voxels in an intra-vital image of the biofilm at day 0 before initiating treatment, using the COMSTAT plug-in in Image J (NIH Research Services Branch, USA).

Immediately prior to sacrifice, blood samples were collected from all mice for biochemical analysis. After sacrifice, abdominal, intra-vital windows were removed and tissue surrounding the window was excised and weighted. Average weight of excised tissue was 0.9 g. Half of the excised tissue was homogenized in PBS. The homogenate was serially diluted, and spread over the TSB agar plates. After 24 h of growth at 37 °C, numbers of CFUs were enumerated. The other half of the excised tissue as well as of the heart, liver, spleen, lung and kidney tissues were fixed in 10% formaldehyde, embedded into paraffin, cut in sections, and stained with hematoxylin-eosin (H&E) for microscopic examination

(Olympus, BX63, Germany).

2.13. Statistical analysis

All data were expressed as means ± SD values. Differences between groups were examined for statistical significance with a one-way ANOVA test. Differences were considered significant at $p < 0.05$.

3. Results

3.1. Mesoporous Fe_3O_4@SiO_2 nanoparticles as a reaction container

TEM micrographs showed that the Fe_3O_4@SiO_2 nanoparticles were spherically shaped, with relatively small, magnetic Fe_3O_4 nanoparticles encapsulated by a relatively thick shell of SiO_2 to yield a mesoporous, composite nanoparticle with a total diameter of around 60 nm (Fig. 1a). Magnetic properties of mesoporous Fe_3O_4@SiO_2 nanoparticles were confirmed by magnetic separation of nanoparticles in suspension (see Fig. 1a, inset) and measurement of their magnetization (Fig. 1b). A wide-scan XPS spectrum of the Fe_3O_4@SiO_2 nanoparticles demonstrated clear Si_{2p} and O_{2p} electron binding energy peaks (Fig. 1c). The Fe_{2p} peak could only be discerned weakly in a narrow-scan over the binding energy range from 700 to 740 eV, confirming their localization inside a shell of SiO_2 nanoparticles with a thickness that exceeds the mean electron free path in the capsular material. N_2 adsorption-desorption isotherms (Fig. 1d) yielded a large surface area (667 m^2 g^{-1}) of the Fe_3O_4@SiO_2 nanoparticles with pores possessing diameters of around 2.9 nm.

3.2. Mesoporous Fe_3O_4@SiO_2 nanoparticles with coupled glucose-oxidase and loaded with L-arginine

Glucose-oxidase (GOx) was covalently coupled onto the surface of magnetic mesoporous Fe_3O_4@SiO_2 nanoparticles by dehydration condensation between the Si–OH groups and APTES-GOx (see Fig. 2 for ^{1}H NMR spectrum of APTES-GOx). L-arginine was loaded into the mesoporous Fe_3O_4@SiO_2 nanoparticles by exposure to an L-arginine solution under gentle magnetic stirring.

APTES-mediated coupling of glucose-oxidase nor additional loading with L-arginine affected the size of Fe_3O_4@SiO_2 nanoparticles (compare Fig. 3a with Fig. 1a). Also, magnetic properties of the nanoparticles remained unaltered (Fig. S4). FTIR absorption spectroscopy (Fig. 3b) demonstrated characteristic absorption bands of Fe_3O_4@SiO_2 at 1083 cm^{-1} and 956 cm^{-1} due to stretching of Si–O–Si and Si–O–H bonds, respectively and a characteristic band due to Fe–O stretching at 578 cm^{-1}. Absorption bands of glucose-oxidase included 3302 cm^{-1} due to -NH- stretching, 3064 cm^{-1} due to O–H stretching, 1634 cm^{-1} due to C═O stretching in amide and 1530 cm^{-1} due to -NH- vibration in amide. Effective coupling of glucose-oxidase onto mesoporous Fe_3O_4@SiO_2 nanoparticles can be concluded from the occurrence of absorption bands characteristic to glucose-oxidase due to -NH- stretching (3296 cm^{-1}), C═O stretching (1643 cm^{-1}), and -NH- deformation (1537 cm^{-1}) after coupling. Coupling occurred through Si–O–Si bridges between Fe_3O_4@SiO_2 and APTES-GOx, as evidenced from a chemical shift in silicon atoms in Fe_3O_4@SiO_2 nanoparticles from −66.0 ppm to −58.5 ppm and −49.0 ppm (see Fig. 3c). FTIR absorption bands of L-arginine were located at 3306 cm^{-1} due to -NH- stretching, 3066 cm^{-1} due to O–H stretching and encompassed a broad range of bands between 1450 cm^{-1} and 1700 cm^{-1} due to C═N stretching in guanidine groups. All L-arginine bands were preserved in the FTIR spectrum of mesoporous Fe_3O_4@SiO_2 nanoparticles with coupled glucose-oxidase and loaded

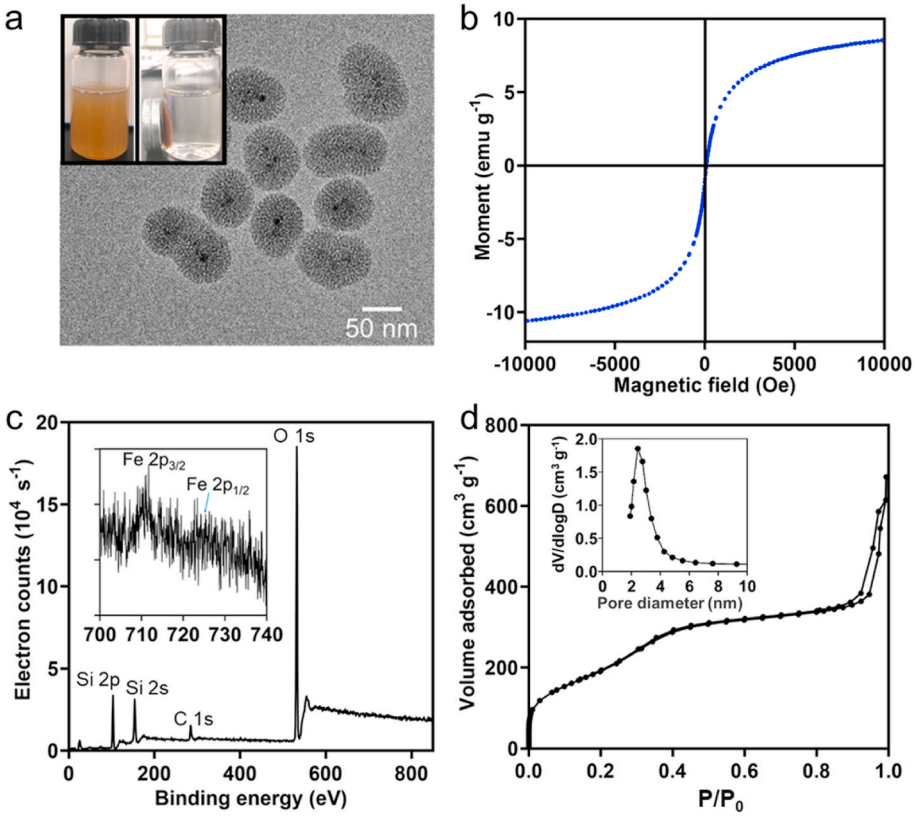

Fig. 1. Mesoporous Fe_3O_4@SiO_2 nanoparticle characterization. (a) TEM micrograph of Fe_3O_4@SiO_2 nanoparticles and demonstration of their magnetic separation from suspension. **(b)** Magnetization curve of Fe_3O_4@SiO_2 nanoparticles. **(c)** Photo-electron binding energy spectrum of Fe_3O_4@SiO_2 nanoparticles, with the inset showing the Fe_{2p} electron binding energy peak. **(d)** N_2 adsorption-desorption isotherms and pore-size distribution of mesoporous Fe_3O_4@SiO_2 nanoparticles.

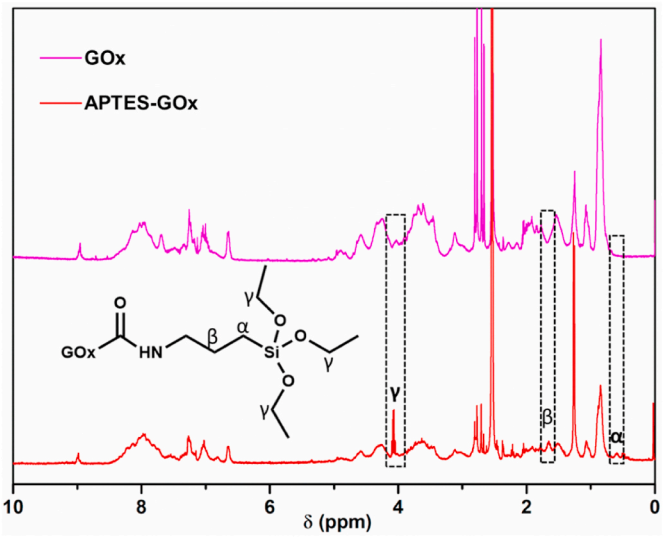

Fig. 2. ^{1}H NMR spectra of GOx and APTES-GOx. Conjugation in APTES-GOx occurred through carboxyl groups in glucose-oxidase with amine groups in APTES and was evidenced by chemical shifts of glucose-oxidase between 0.82 and 4.86 ppm due to hydrogens in methyl, methylene, methine groups, together with a number of chemical shifts between 6.64 and 8.95 ppm due to hydrogens in aromatic and amide groups. In addition, conjugation was evidenced by a new chemical shift at 0.57 ppm of the **α** hydrogens, at 1.62 ppm of **β** hydrogens and at 4.05 ppm of **γ** hydrogens in APTES. Chemical shifts of other types of hydrogens in APTES merged with that in glucose-oxidase.

with L-arginine (see also Fig. 3b). Thermographic analyses confirmed coupling of glucose-oxidase and loading with L-arginine and weight loss analyses indicated 11% coupling of glucose-oxidase and 13% loading of L-arginine (Fig. 3d).

Generation of H_2O_2 and NO was subsequently quantified using a Hydrogen Peroxide Assay Kit and Griess reagent, respectively based on the UV–vis absorbances of H_2O_2 after reaction with the Hydrogen Peroxide Assay Kit components (at 560 nm) and reaction of NO with Griess reagent (at 540 nm). Respective standard curves are shown in (Figs. S1a and S1b). H_2O_2 generation by Fe_3O_4@SiO_2 nanoparticles with coupled glucose-oxidase according to the reaction I (Scheme 1) increased with increasing glucose concentration (Fig. 4a). Also, NO generation by mesoporous Fe_3O_4@SiO_2 nanoparticles with coupled glucose-oxidase and additional loading with L-arginine according to the reaction II (Scheme 1) increased with increasing glucose concentration (Fig. 4b). NO generation at a physiological glucose concentration of 800 μg mL^{-1} was higher at pH 5.0 than at pH 7.4 (Fig. 4c), likely because H_2O_2 generation is accompanied by the generation of gluconic acid in the first cascade reaction. Since oxidization of L-arginine by H_2O_2 is enhanced at acidic pH (Fig. S5), the generation of gluconic acid enhanced the generation of NO in the second cascade reaction.

H_2O_2 generated in the first cascade reaction can not only serve to oxidize L-arginine to generate NO, but potentially might also be catalyzed by Fe_3O_4 located in the inner core of Fe_3O_4@SiO_2 nanoparticles to yield •OH through a Fenton reaction [25]. However, •OH generation was extremely small, both at pH 5.0 (Fig. S2f) and pH 7.4 (Fig. S2g), likely because H_2O_2 diffusion through the mesoporous silica shell to the Fe_3O_4 inner core was small.

3.3. Killing efficacy of mesoporous Fe_3O_4@SiO_2 nanoparticles with coupled glucose-oxidase and loaded with L-arginine against planktonic bacteria

Two Gram-positive (*S. aureus* ATCC12600^{GFP} and *S. aureus* Xen36) and one Gram-negative (*E. coli* Xen14) bacterial strains were used for determining the killing efficacy of mesoporous Fe_3O_4@SiO_2 nanoparticles with coupled glucose-oxidase and loaded with L-arginine. Based on their Minimal Inhibitory Concentrations (see Table S4), all three strains can be classified as vancomycin-resistant. Vancomycin-resistance was confirmed by comparing growth of planktonic staphylococci (Fig. 5a and b) or *E. coli* Xen14 (Fig. 5c) in PBS and in PBS with vancomycin added, demonstrating no significant differences irrespective of time. Note, that planktonic growth of the *S. aureus* strain with the lowest MIC (*S. aureus* ATCC12600^{GFP}) in presence of vancomycin showed a minor reduction with respect to PBS. Coupling only glucose-oxidase to the nanoparticles led to a significant, time-dependent reduction in CFUs, that amounted 3 to 5 log-units reduction ($p < 0.0001$, one-way ANOVA) with respect to vancomycin after 6 h. These reductions must be attributed to the production of H_2O_2 in the first cascade-reaction. Loading with L-arginine in absence of GOx-coupling however, did not yield any reduction in CFUs as compared with vancomycin, neither in staphylococci nor in *E. coli*, because H_2O_2 as required for the second cascade-reaction was absent. However, GOx-coupling combined with L-arginine loading of the nanoparticles, yielded significantly stronger reduction as compared with vancomycin at all points in time and for all three strains. Moreover, GOx-coupling combined with L-arginine yielded slightly stronger reductions at all time points with respect to GOx-coupling in all three strains due to conversion of H_2O_2 into NO in the second reaction of the cascade (see Scheme 1). Reductions upon additional loading with L-arginine were only slightly stronger than for GOx-loading due to the generation of NO at distances between the generation site and planktonic target bacteria that could not be bridged by diffusion within the life-time of NO.

3.4. Targeting of magnetic cascade-reaction containers and eradication of infectious biofilms in vitro

Evaluation of the efficacy of magnetic cascade-reaction containers towards an infectious biofilm requires application of a magnetic field to establish even distribution of magnetic cascade-reaction containers over the depth of a biofilm. Since it has recently been demonstrated [20] that this critically depends on the magnetic field strength and targeting time applied to prevent over- and under-accumulation of magnetic nanoparticles near the top or bottom of a biofilm, we first determined optimal magnetic targeting conditions. To this end, green-fluorescent *S. aureus* ATCC12600^{GFP} biofilms (average thickness 82 μm, coinciding with the thickness of many clinically occurring biofilms [26] were exposed to red-fluorescent Rhodamine-B labeled magnetic reaction containers (Fig. 6a). Analysis of the distribution of red-fluorescent cascade-reaction containers over the depth of a staphylococcal biofilm (Fig. 6b) demonstrated accumulation near the top of the biofilm for short magnetic field exposure times (5 and 10 min, Fig. 6c and d). Reaction containers were driven to the bottom of the biofilm at the expense of their presence in the top region, when exposure times were increased to 60 min (Fig. 6f). 30 min magnetic field exposure yielded the most homogeneous in-biofilm distribution of magnetic cascade-reaction containers over the depth of a biofilm (Fig. 6e) and was used in all further experiments.

Neither Gram-positive *S. aureus* nor Gram-negative *E. coli* were eradicated in thick biofilms upon exposure to vancomycin or after magnetic-targeting of reaction containers only loaded with L-arginine (Fig. 7). Time-dependent killing was observed after magnetic-targeting of reaction containers with only coupled glucose-oxidase within 6 h, leading to a significant bacterial killing in biofilms with respect to vancomycin after 6 h ($p < 0.0001$, one-way ANOVA). Interestingly, magnetic reaction containers with coupled glucose-oxidase and loaded with L-arginine in absence of magnetic targeting yielded a similar killing as did reaction containers with coupled glucose-oxidase only. This demonstrates that the H_2O_2 generated in the first cascade-reaction has the ability to diffuse in the biofilm to kill its inhabitants, while oppositely the NO generated outside a biofilm in the second cascade-reaction may not be sufficiently long-lived to diffuse into the biofilm and kill its bacterial inhabitants. This suggestion is confirmed by the observation

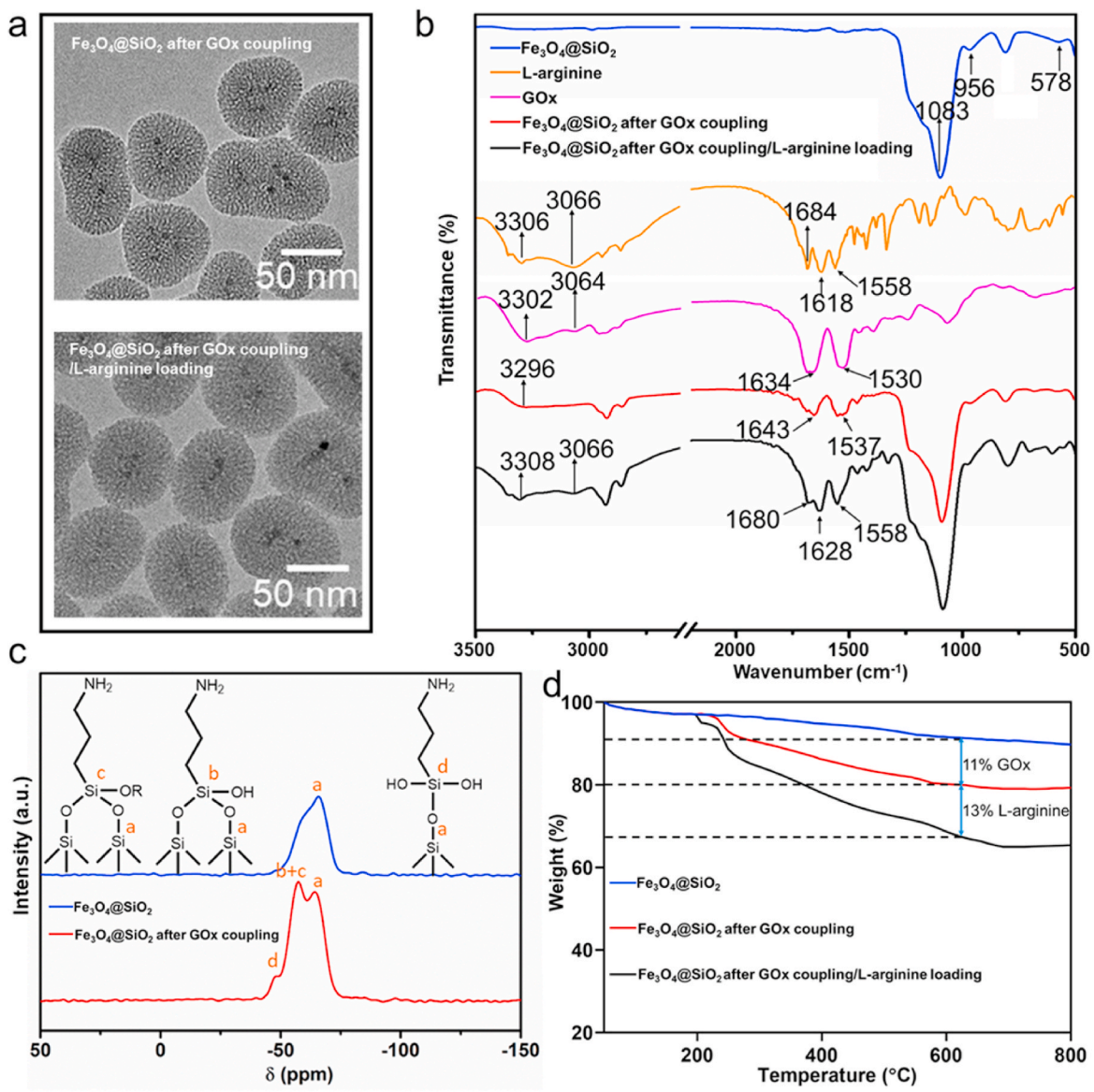

Fig. 3. Mesoporous Fe_3O_4@SiO_2 nanoparticles with coupled glucose-oxidase and loaded with L-arginine. (a) TEM micrographs of Fe_3O_4@SiO_2 nanoparticles after coupling of glucose-oxidase and additional loading with L-arginine. **(b)** FTIR absorption spectra of Fe_3O_4@SiO_2 nanoparticles, L-arginine, glucose-oxidase, Fe_3O_4@SiO_2 nanoparticles with coupled glucose-oxidase and after additional loading with L-arginine. **(c)** ^{29}Si NMR spectrum of Fe_3O_4@SiO_2 nanoparticles before and after APTES-mediated coupling of glucose-oxidase. **(d)** Percentage weight loss as a function of temperature of Fe_3O_4@SiO_2 nanoparticles before and after coupling of glucose-oxidase and additional loading with L-arginine.

that magnetic cascade-reaction containers with coupled glucose-oxidase and loaded with L-arginine yielded significantly better killing upon magnetic targeting at all time points and in all three strains (Fig. 7), both with respect to vancomycin as well as with respect to nanoparticles with only coupled GOx or only L-arginine loading. Thus, in-biofilm generation of NO is a *conditio sine qua non* for eradicating infectious biofilms.

3.5. *Targeting and eradication of an intra-abdominal biofilm by magnetic cascade-reaction containers observed through an intra-vital window in living mice*

Before doing animal experiments, it was first ascertained that the hemolytic activity of Fe_3O_4@SiO_2 cascade-reaction containers was negligible and cytotoxicity absent at the concentrations used for *in vivo* experiments. Hemolysis was concentration dependent (Fig. S6) and less than the medical adsorbent standard of 5% (ISO 10993.4:2002) [27] at the highest nanoparticle concentration used *in vivo* (800 μg mL^{-1}). Cytotoxicity of Fe_3O_4@SiO_2 cascade-reaction containers towards mouse embryonic fibroblasts was small (Fig. S7), although increasing with increasing concentration of cascade-reaction containers. After 24 h exposure fibroblasts had maintained 62% viability at 1200 μg mL^{-1}. Considering a critical threshold of 30%–40% suggested for maintaining tissue cell integration [28] this may be considered high and acceptable.

Magnetic targeting of red-fluorescent Rhodamine-B labeled cascade-reaction containers in mice was done by real-time observation through an abdominal, intra-vital window implanted in the flanks of mice, underneath which a green-fluorescent *S. aureus* ATCC12600^{GFP} biofilm was grown (Fig. 8a). Bioluminescence imaging showed that in absence of magnetic targeting, cascade-reaction containers diffused slowly over time from their injection site over the entire body of the mice, without major accumulation in the biofilm. Some accumulation was observed after 1 and 6 h in the region around the liver and spleen (Fig. 8b). Upon sacrifice of mice at 24 h however, bioluminescence imaging indicated no accumulation in any region of the body. Magnetic targeting yielded

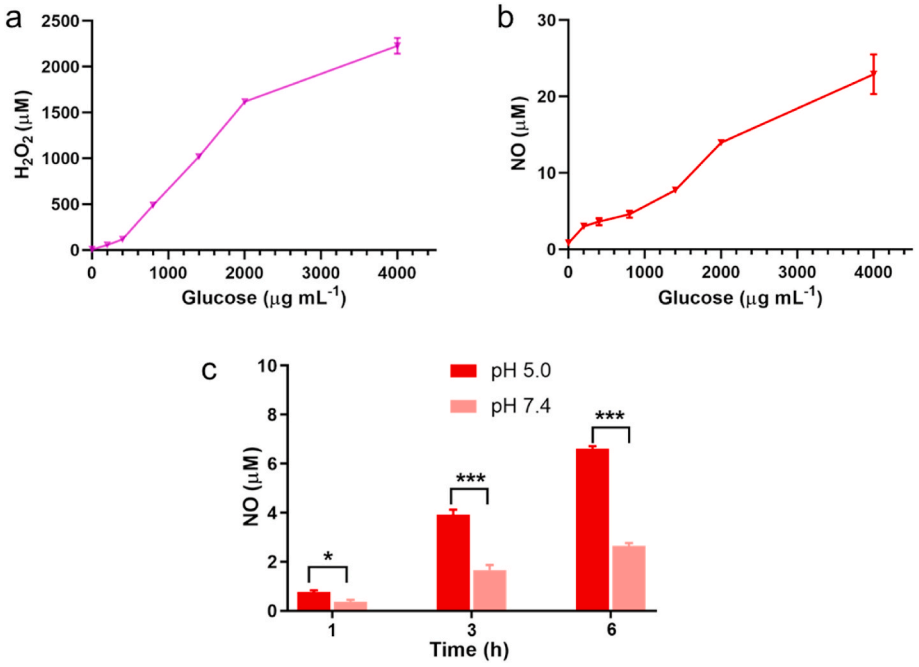

Fig. 4. Enzyme activity of mesoporous Fe_3O_4@SiO_2 nanoparticles suspended in PBS (300 μg mL^{-1}) after glucose-oxidase coupling and additional L-arginine loading. (a) The amount of H_2O_2 generated at pH 5.0 through Fe_3O_4@SiO_2 nanoparticles with coupled glucose-oxidase as a function of the glucose concentration according to Reaction I (Scheme 1). Note the glucose concentration range applied encompassed the physiological glucose concentration (630–990 μg mL^{-1}) [24]. For measurement, 500 μL of a nanoparticle suspension was mixed for 3 h with 500 μL Hydrogen Peroxide Assay Kit reagent at 37 °C in the dark. **(b)** The amount of NO generated at pH 5.0 by Fe_3O_4@SiO_2 nanoparticles with coupled glucose-oxidase and additional loading with L-arginine as a function of the glucose concentration, according to Reaction II (see also Scheme 1). For measurement, 500 μL of a nanoparticle suspension was mixed for 3 h with 500 μL Griess reagent (equal amounts of reagent I and II) at 37 °C in the dark. **(c)** A comparison of the amount of NO generated through Fe_3O_4@SiO_2 nanoparticles with coupled glucose-oxidase and additional loading with L-arginine as a function of time at a glucose concentration of 800 μg mL^{-1} and different pH. Other conditions and methods as in panel (b). All data represent means±standard deviations over triplicate runs with separately prepared nanoparticles batches. * and *** indicate statistical significances at $p < 0.05$ and $p < 0.001$, respectively (Student's *t*-test).

accumulation of cascade-reaction containers in the biofilm underneath the intra-vital window within 1 h (Fig. 8b and Movie S1). This accumulation increased up to a maximum, that was reached after 6 h, i.e. slightly after arresting of magnetic field application. Accumulation of cascade-reaction containers in the biofilm underneath the intra-window upon application of a magnetic field was three-fold higher at 6 h than in absence of a magnetic field (Fig. 8c). High accumulation in the biofilm underneath the intra-vital window remained observable through bioluminescence imaging at sacrifice of mice at 24 h. Accumulation of RhB-labeled magnetic cascade-reaction containers in the liver and spleen in absence of magnetic targeting was confirmed by fluorescence-analyses of organ tissues in mice sacrificed at different time points (Fig. S8a). Fluorescence-analyses also confirmed absence of accumulation in tissue surrounding the intra-vital window. In presence of magnetic targeting however, fluorescence-analyses indicated three-fold higher accumulation in surrounding tissue at all points in time than measured in absence of magnetic targeting (compare Fig. S8a and Fig. S8b). In addition, fluorescence in liver and spleen tissues was confirmed to be smaller after magnetic targeting due to directing of magnetic cascade-reaction containers from the blood circulation towards the infection site.

Supplementary data related to this article can be found at https://doi.org/10.1016/j.bioactmat.2022.01.044.

Longer term analysis extending over six days (see Fig. 8d for scheme) using two-photon confocal laser scanning microscopic imaging of staphylococcal biofilms underneath the intra-vital window (Fig. 8e), demonstrated minor reductions in biomass over time during treatment with vancomycin ($p < 0.05$, one-way ANOVA) or magnetic cascade-reaction containers at 800 μg mL^{-1} in absence of magnetic targeting ($p < 0.01$, one-way ANOVA) (Fig. 8f). Also tissue surrounding the intra-vital window that had become infected during biofilm growth or treatment and collected at sacrifice, contained less staphylococcal CFUs in the groups of mice treated with vancomycin ($p < 0.05$, one-way ANOVA) or magnetic cascade-reaction containers in absence of magnetic targeting ($p < 0.01$, one-way ANOVA) than in the group injected with PBS (Fig. 8f).

Superior eradication of the intra-abdominal biofilm was observed however, when magnetic cascade-reaction containers were targeted into the biofilm by placing a magnet on the intra-vital window, both with respect to biomass (Fig. 8f) as well as with respect to the number of CFUs in tissue surrounding the window (Fig. 8g). Use of a lower concentration of magnetic cascade-reaction containers than 800 μg mL^{-1} yielded significantly less reduction in biomass (Fig. S9a) and CFUs (Fig. S9b), while the added value of a higher concentration was small and at the expense of blood compatibility (Fig. S6) and tissue cell viability (Fig. S7). Eradication of intra-abdominal biofilms was confirmed through histological analysis of tissue surrounding the intra-vital window taken at sacrifice, showing a near intact epidermis structure and few inflammatory cells in mice with magnetic cascade-reaction containers targeted into the biofilm (Fig. S10). In line, analysis of blood extracted at sacrifice, showed minor ($p < 0.05$ one-way ANOVA) increases in white blood cell counts upon injection of PBS, vancomycin or reaction containers in absence of magnetic targeting (Fig. S11), but white blood cells counts in the group of mice treated with magnetically targeted reaction containers were similarly low as in uninfected mice. Other blood parameters were similar in all groups (see also Fig. S11). Histological analyses of organ tissues taken at sacrifice (day 6) demonstrated no adverse effects in heart, liver, spleen, lung and kidney tissue across all groups of mice (Fig. S12). This demonstrates that the small accumulation of cascade-reaction containers after magnetic targeting in liver and spleen tissue (Fig. S8b) observed 24 h after injection, was biologically insignificant on the longer term.

4. Discussion

A cascade-reaction container composed of magnetic, mesoporous Fe_3O_4@SiO_2 nanoparticles containing glucose-oxidase and L-arginine was designed that could be magnetically targeted inside an infectious biofilm. Glucose-oxidase generated H_2O_2 at endogenous glucose concentrations, while subsequently L-arginine generated NO in a second cascade-reaction from the H_2O_2 generated in the first reaction.

These magnetically-targeted cascade-reaction containers killed both Gram-positive and Gram-negative bacteria and were demonstrated to kill *S. aureus* in an abdominal biofilm in mice after tail-vein injection and

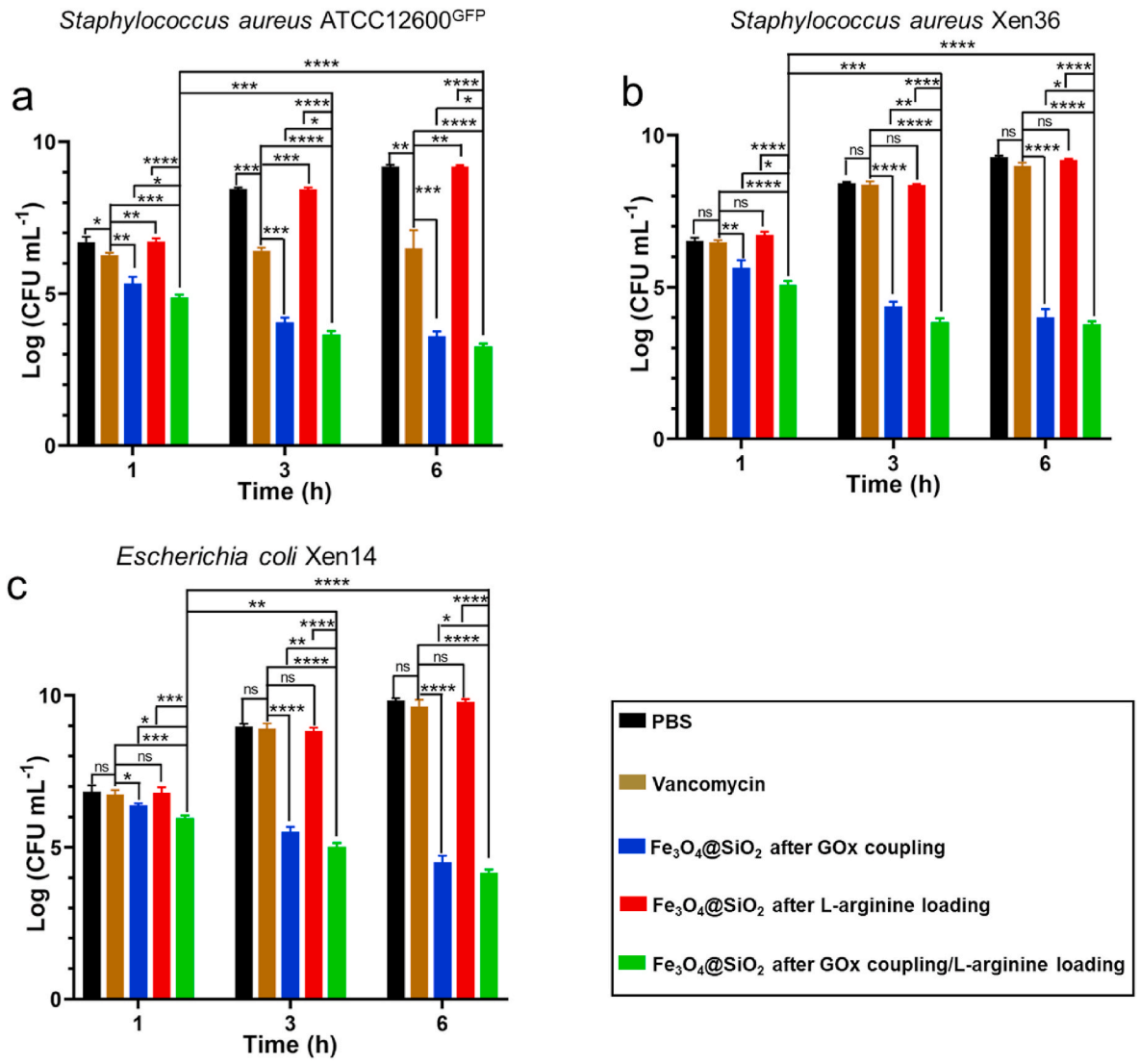

Fig. 5. Killing efficacy of mesoporous Fe_3O_4@SiO_2 nanoparticles with coupled glucose-oxidase and loaded with L-arginine against planktonic bacteria. Experiments were carried out with Gram-positive *S. aureus* or Gram-negative *E. coli* strains suspended (1×10^6 bacteria mL^{-1}) in TSB or LB, respectively supplemented with glucose to a final concentration 800 μg mL^{-1}. Fe_3O_4@SiO_2 nanoparticles or vancomycin were added to a final concentration of 80 μg mL^{-1} or 5 μg mL^{-1}, respectively. Aliquots were taken at different points in time for CFU enumeration. PBS was taken as a control. **(a)** Log (CFU mL^{-1}) of *S. aureus* ATCC12600^{GFP} after growth in the presence of nanoparticles or vancomycin. **(b)** Same as panel (a), now for *S. aureus* Xen36. **(c)** Same as panel (a), now for *E. coli* Xen14. Data represent averages over 3 replicates over separately prepared batches of nanoparticles and different bacterial cultures. Error bars indicate standard deviations. *, **, *** and **** indicate statistical significances at $p < 0.05$, $p < 0.01$, $p < 0.001$ and $p < 0.0001$ for the comparisons indicated by the spanning bars (one-way ANOVA).

magnetic targeting of the cascade-reaction containers into the biofilm. Eradication of an abdominal biofilm could be achieved consuming only endogenous glucose, without adding any additional glucose. Delineation of the killing efficacies of the first and second cascade reaction yielded the conclusion that NO generation in the second cascade-reaction did not enhance killing of planktonic bacteria in suspension viz a viz bacterial killing by the H_2O_2 generated in the first cascade-reaction in microbiologically significant numbers, although a minor, statistically significant reduction was observed. However, in-biofilm generation of NO after magnetic targeting of the cascade-reaction containers in a biofilm was essential for maximal killing of Gram-positive and Gram-negative bacteria in a biofilm-mode of growth. Compared with vancomycin, magnetic, mesoporous Fe_3O_4@SiO_2 nanoparticles containing glucose-oxidase and L-arginine yielded 4–5 log-units better killing of planktonic *S. aureus* and *E. coli* (Fig. 5), 2–3 log-units better killing of strains in a biofilm-mode of growth (Fig. 7) and 1–2 log-units better killing than vancomycin *in vivo* (Fig. 8g).

Many nano-antimicrobials rely on the generation of ROS for bacterial killing, but mostly generate ROS from externally added oxygen-species, like externally added H_2O_2 [29–31]. Suitable oxygen-species are not readily available in sufficiently high concentrations near an infection site in the human body. In the liner enzyme cascade-reaction proposed, H_2O_2 is generated from glucose that is readily available in the human body. Subsequently, the combination of GOx and L-arginine not only consumes glucose to generate H_2O_2, but also generates NO, one of the ROS with a relatively long life-time, i.e. 0.09–2 s [22]. A life-time of 0.09–2 s, will allow NO to diffuse around 25–115 μm in aqueous solution [32]. All cascade-reaction containers described in the literature, generate OH radicals with an approximate life-time of 3.7×10^{-9} s, allowing OH radicals to diffuse around 60 Å in aqueous solution [33]. This is too short to bridge the distance between a generation site and a target bacterium in suspension, particularly at low substrate, container and bacterial concentrations. As a consequence, the efficacy of these systems for killing planktonic bacteria is relatively low, unless extremely high concentrations of glucose are added (see Table S1) far above the toxic limit to humans [34]. Our GOx, L-arginine based cascade reaction

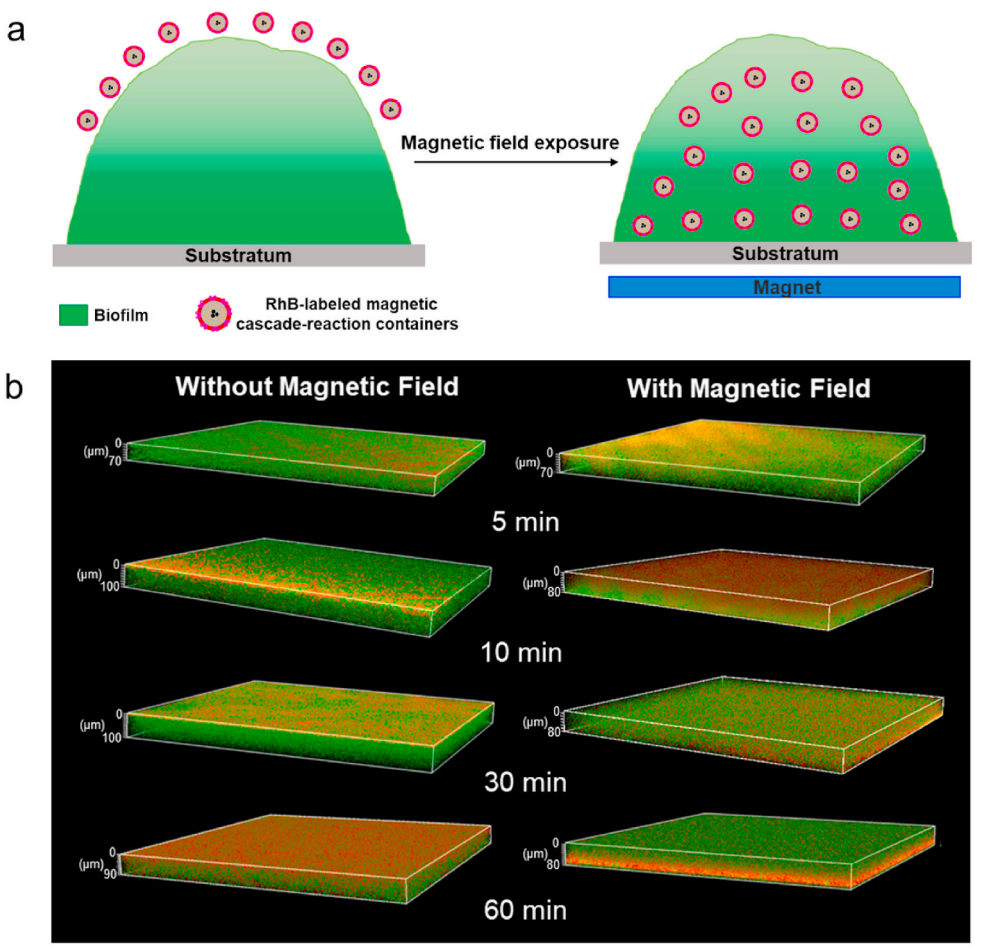

Fig. 6. Determination of optimal magnetic targeting time to establish even in-biofilm distribution of magnetic cascade-reaction containers over the depth of a biofilm *in vitro*. **(a)** Schematics of targeting of Rhodamine-B (RhB) labeled, magnetic cascade-reaction containers to an in vitro *S. aureus* ATCC12600^{GFP} biofilm. **(b)** 3D-CLSM micrographs of green-fluorescent *S. aureus* ATCC12600^{GFP} biofilms exposed to red-fluorescent magnetic cascade-reaction containers suspended in PBS (100 μg mL^{-1}) after different magnetic field exposure times. **(c)** Normalized red-fluorescence due to penetration and accumulation in biofilms as a function of the depth in the biofilm after 5 min magnetic field exposure, as calculated from CLSM micrographs (see Fig. 6b). Red-fluorescence intensity was normalized with respect to the maximum fluorescence intensity observed across all images taken. **(d)** Same as panel (c), now for 10 min magnetic field exposure. **(e)** Same as panel (c), now for 30 min magnetic field exposure. **(f)** Same as panel (c), now for 60 min magnetic field exposure.

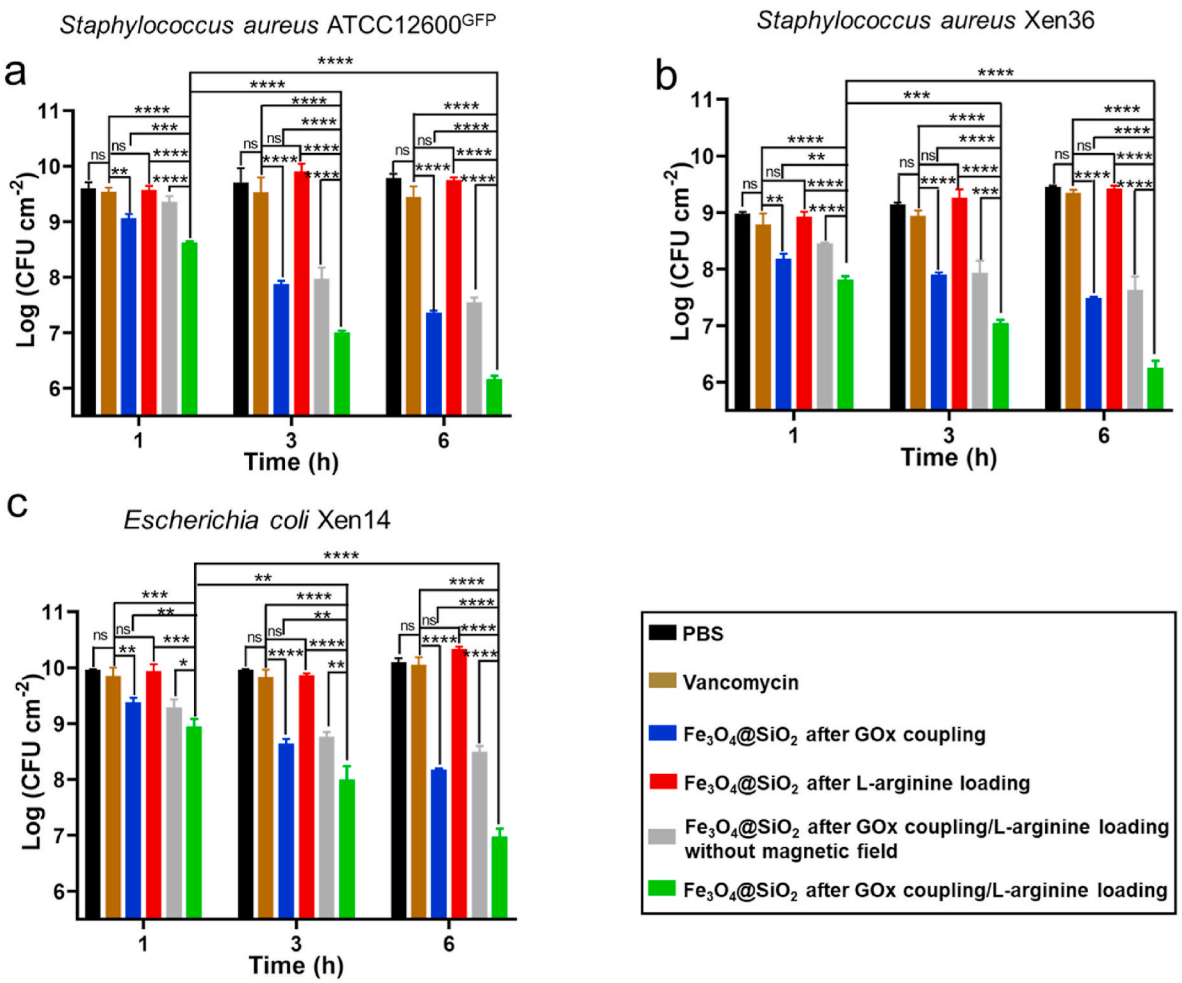

Fig. 7. Killing efficacy of magnetic cascade-reaction containers with coupled glucose-oxidase and loaded with L-arginine against bacteria in a biofilm-mode of growth. Experiments were carried out with bacterial biofilms grown in TSB or LB, supplemented with glucose to a final concentration 800 μg mL^{-1}. Biofilms were grown for 48 h to an average thickness of 82 μm. After growth, biofilms were exposed to PBS (control), vancomycin in solution (10 μg mL^{-1}) or cascade-reaction containers (300 μg mL^{-1}) under 30 min magnetic field application. **(a)** Biofilms of *S. aureus* $ATCC12600^{GFP}$. **(b)** Biofilms of *S. aureus* Xen36. **(c)** Biofilms of *E. coli* Xen14. Data represent averages over 3 replicates over separately prepared batches of nanoparticles and different bacterial biofilms. Error bars indicate standard deviations. *, **, *** and **** indicate statistical significances at $p < 0.05$, $p < 0.01$, $p < 0.001$ and $p < 0.0001$ (one-way ANOVA).

containers moderately killed planktonic bacteria in presence of 800 μg mL^{-1} glucose, within the range of healthy glucose levels [24]. Only one study on cascade-reaction containers based on calcium peroxide nanoparticles with Ag NPs allowed comparison of its efficacy against bacteria in a biofilm-mode with our GOx/L-arginine based cascade-reaction containers (see Table S2). Magnetic, mesoporous GOx/L-arginine based cascade reaction containers were 1–2 log-units more effective in killing biofilm bacteria after magnetic targeting than calcium peroxide nanoparticles with Ag NPs, although reductions were not expressed in directly comparable units (see Table S2). In absence of magnetic targeting, GOx/L-arginine based cascade reaction containers had a similar killing efficacy towards biofilm bacteria as did reaction containers solely loaded with GOx. Hence, it can be concluded that the NO generated only contributes to the killing of biofilm bacteria provided generation occurs in-biofilm.

Efficacy of glucose consuming cascade-reaction containers *in vivo* (see Table S3) has only been studied using infected wounds in mice, with the exception of the present study that is based on an abdominal biofilm model. None of the OH-radicals based cascade-reaction containers yielded meaningful reductions in CFUs in an infected wound model, neither in diabetic mice nor in healthy mice unless a high dose of glucose was administered at the same time (see Table S3). Our magnetic, mesoporous $Fe_3O_4@SiO_2$ with coupled GOx and loaded with L-arginine performed better in an abdominal biofilm model without glucose addition than Cu-TCPP(Fe) nanosheets in an infected wound model while adding a high dose of glucose (see Table S3). This points to the advantage of NO-based cascade-reactions requiring only endogenous glucose, naturally present in healthy patients.

The use of abdominal biofilms with an intra-vital window to visualize biofilm targeting and eradication by nano-antimicrobials has only been applied for pH-responsive, self-targeting micelles [35] and liposomes [36], but not yet for magnetic targeting of cascade-reaction containers. Interestingly, despite the problems in finding magnetic field conditions for evenly distributing magnetic cascade-reaction containers over the depth of a biofilm using a one-directional, single magnet (Fig. 6), *in vivo* targeting of an abdominal biofilm turned out to be surprisingly simple (Fig. 8 and Movie S1) and effective to enhance bacterial killing. One-directional, single-magnets to attract magnetic nanoparticles to an infection site have been used before in small animal models [37], but likely targeting of a micron-sized biofilm may be much more difficult in larger sized mammals. Up to what extent this will affect clinical translation of the use of magnetic, cascade-reaction containers as a new, non-antibiotic-based infection-control strategy remains to be seen. Current multiple-magnet systems consisting of several electromagnets arranged in a spatial array [38] may allow 3D targeting with micrometer resolution in deep tissues, required for biofilm targeting in

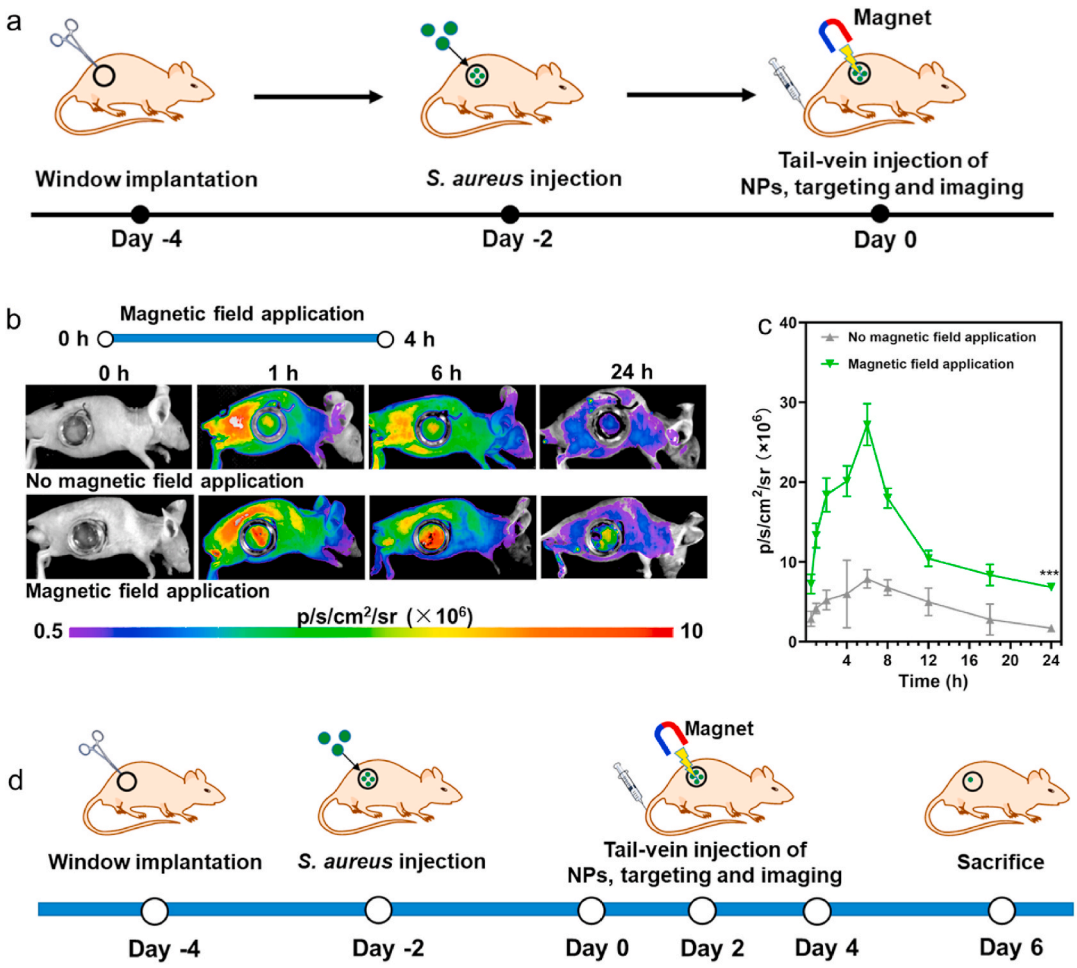

(caption on next page)

Fig. 8. Targeting and accumulation of magnetic cascade-reaction containers in an abdominal *S. aureus* biofilm underneath an intra-vital window in living mice and biofilm eradication. (a) Time-line of events for monitoring magnetic targeting of reaction containers to an abdominal *S. aureus* ATCC12600^{GFP} biofilm. After abdominal biofilm growth for 2 days, mice were tail-vein injected with 200 μL of a suspension of Rhodamine-B (RhB) labeled cascade-reaction containers in PBS (800 μg mL^{-1}) and exposed to a magnetic field over the intra-vital window for 4 h. **(b)** Distribution of red-fluorescent RhB-labeled magnetic cascade-reaction containers through the body of a mouse imaged using bioluminescence imaging, in presence and absence of an applied magnetic field. **(c)** Red-fluorescence intensity due to RhB-labeled magnetic cascade-reaction containers accumulated in staphylococcal biofilms underneath an intra-vital window in mice as a function of time, corresponding to panel (b). **(d)** Time-line of events for monitoring eradication of an abdominal *S. aureus* ATCC12600^{GFP} biofilm underneath an intra-vital window in living mice. After abdominal biofilm growth, mice were tail-vein injected with 200 μL of PBS, vancomycin in solution (500 μg mL^{-1}) or magnetic cascade-reaction containers (800 μg mL^{-1}) followed by magnetic field exposure during 4 h. Injection and magnetic targeting was repeated at days 2 and 4. **(e)** Examples of reconstructed 3D-intra-vital images of green-fluorescent *S. aureus* ATCC 12600^{GFP} biofilms underneath an intra-vital window in living mice before initiating treatment at day 0 and after tail-vein injection of 200 μL of PBS (0 μg mL^{-1}) or PBS with suspended magnetic cascade-reaction containers (800 μg mL^{-1}). **(f)** Staphylococcal biomass underneath an intra-vital window in mice as a function of time after initiating treatment in presence and absence of an applied magnetic field over the intra-vital window, derived from COMSTAT analysis of intra-vital images. **(g)** Number of *S. aureus* CFUs per g tissue excised from around the intra-vital window site after sacrifice at day 6 after initiating treatment. Error bars denote standard deviations over 3 mice. *, ** and **** indicate statistical significances at $p < 0.05$, $p < 0.01$ and $p < 0.0001$ (one-way ANOVA test).

humans.

5. Conclusions

A magnetic, liner cascade-reaction container was made, consisting of mesoporous Fe_3O_4@SiO_2 nanoparticles containing glucose-oxidase and L-arginine. Under the application of a suitable external magnetic field, magnetic cascade-reaction containers could be homogeneously distributed across the depth of an infectious biofilm in vitro and accumulated within 6 h after tail-vein injection inside an abdominal biofilm, as observed real-time in living mice with an implanted intra-vital window. Magnetic targeting and distribution across the depth of an infectious biofilm was necessary to benefit from L-arginine-assisted NO generation in the second cascade-reaction, consuming the H_2O_2 generated using glucose-oxidase in the first cascade-reaction. This in-biofilm generation of NO is necessary to benefit optimally from both reactions in the cascade. Mesoporous Fe_3O_4@SiO_2 nanoparticle reaction containers with GOx/L-arginine neither caused hemolysis not adverse blood or organ tissue reactions, making them suitable for use against infectious Gram-positive and Gram-negative biofilms, provided suitably targeted inside a biofilm. For clinical use in humans, it is important to realize that higher doses should be applied than used in our murine study. In our murine, we successfully applied an injection of 200 μL at a concentration of 800 μg mL^{-1}. Considering humans have about 5 L of blood *versus* 2×10^{-3} L of blood in a mouse, the dose should be 2500-fold higher, which can be achieved by increasing either the concentration or the volume injected. Important for potential clinical use as well, Fe_3O_4@SiO_2 nanoparticle reaction containers with GOx/L-arginine eradicate infectious biofilms without using antibiotics and are effective using endogenous glucose at concentrations present in healthy humans, without addition of glucose. Moreover, efficacy may be higher in diabetic patients due to the presence of higher glucose concentration as a substrate for the cascade to start generation of H_2O_2 and NO.

CRediT authorship contribution statement

Guang Yang: Conceptualization, Investigation, Methodology, Formal analysis, Data curation, Writing – original draft. **Da-Yuan Wang:** Investigation, Methodology, Formal analysis. **Yong Liu:** Validation, Visualization. **Fan Huang:** Validation, Visualization. **Shuang Tian:** Investigation, Methodology, Formal analysis. **Yijin Ren:** Supervision, Writing – review & editing. **Jianfeng Liu:** Writing – review & editing, Funding acquisition. **Yingli An:** Soft-ware, Writing – review & editing. **Henny C. van der Mei:** Conceptualization, Supervision, Writing – review & editing. **Henk J. Busscher:** Conceptualization, Supervision, Writing – review & editing. **Linqi Shi:** Conceptualization, Supervision, Writing – review & editing, Funding acquisition.

Declaration of competing interest

H.J.B. is also director of a consulting company SASA BV. The authors declare no potential conflicts of interest with respect to authorship and/or publication of this article. Opinions and assertions contained herein are those of the authors and are not construed as necessarily representing views of the funding organization or their respective employer (s).

Acknowledgements

This work was financially supported by the National Natural Science Foundation of China (51933006, 21620102005), The Non-profit Central Research Institute Fund of Chinese Academy of Medical Sciences (2018PT35031).

Appendix A. Supplementary data

Supplementary data to this article can be found online at https://doi.org/10.1016/j.bioactmat.2022.01.044.

References

[1] A. Petchiappan, D. Chatterji, Antibiotic resistance: current perspectives, ACS Omega 2 (2017) 7400–7409, https://doi.org/10.1021/acsomega.7b01368.
[2] A. Coates, Y. Hu, R. Bax, C. Page, The future challenges facing the development of new antimicrobial drugs, Nat. Rev. Drug Discov. 1 (2002) 895–910, https://doi.org/10.1038/nrd940.
[3] X. Liu, Z. Yan, Y. Zhang, Z. Liu, Y. Sun, J. Ren, X. Qu, Two-dimensional metal-organic framework/enzyme hybrid nanocatalyst as a benign and self-activated cascade reagent for *in vivo* wound healing, ACS Nano 13 (2019) 5222–5230, https://doi.org/10.1021/acsnano.8b09501.
[4] F. Gao, T. Shao, Y. Yu, Y. Xiong, L. Yang, Surface-bound reactive oxygen species generating nanozymes for selective antibacterial action, Nat. Commun. 12 (2021) 745, https://doi.org/10.1038/s41 467-021-20965-3.
[5] T. Li, J. Li, Q. Pang, L. Ma, W. Tong, C. Gao, Construction of microreactors for cascade reaction and their potential applications as antibacterial agents, ACS Appl. Mater. Interfaces 11 (2019) 6789–6795, https://doi.org/10.1021/acsami.8b20069.
[6] J. Shi, Y. Wu, S. Zhang, Y. Tian, D. Yang, Z. Jiang, Bioinspired construction of multi-enzyme catalytic systems, Chem. Soc. Rev. 47 (2018) 4295–4313, https://doi.org/10.1039/C7CS00914C.
[7] S. Li, H. Cheng, B. Xie, W. Qiu, J. Zeng, C. Li, S. Wan, L. Zhang, W. Liu, X. Zhang, Cancer cell membrane camouflaged cascade bioreactor for cancer targeted starvation and photodynamic therapy, ACS Nano 11 (2017) 7006–7018, https://doi.org/10.1021/acsnano.7b02533.
[8] Y. Li, G. Yang, Y. Ren, L. Shi, R. Ma, H.C. Van Der Mei, H.J. Busscher, Applications and perspectives of cascade reactions in bacterial infection control, Front. Chem. 7 (2020) 861, https://doi.org/10.3389/fc hem.2019.00861.
[9] Z. Yan, W. Bing, C. Ding, K. Dong, J. Ren, X. Qu, A H_2O_2-free depot for treating bacterial infection: localized cascade reactions to eradicate biofilms *in vivo*, Nanoscale 10 (2018) 17656–17662, https://doi.org/10.1039/C8NR03963A.
[10] T. Wang, M.D.J. Libardo, A.M.A. Boza, J.P. Pellois, Membrane oxidation in cell delivery and cell killing applications, ACS Chem. Biol. 12 (2017) 1170–1182, https://doi.org/10.1021/acschembio.7b002 37.
[11] J.A. Imlay, Pathways of oxidative damage, Annu. Rev. Microbiol. 57 (2003) 395–418, https://doi.org/10.1146/annurev.micro.57.030502.090938.
[12] F. Vatansever, W.C.M.A. de Melo, P. Avci, D. Vecchio, M. Sadasivam, A. Gupta, R. Chandran, M. Karimi, N.A. Parizotto, R. Yin, G.P. Tegos, M.R. Hamblin,

Antimicrobial strategies centered around reactive oxygen species-bactericidal antibiotics, photodynamic therapy, and beyond, FEMS Microbiol. Rev. 37 (2013) 955–989, https://doi.org/10.1111/1574-6976.12026.
[13] L. Yang, E.S. Feura, M.J.R. Ahonen, M.H. Schoenfisch, Nitric oxide-releasing macromolecular scaffolds for antibacterial applications, Adv. Healthc. Mater. 7 (2018) 1800155, https://doi.org/10.1002/adhm.201800155.
[14] Y. Li, L. Wang, H. Liu, Y. Pan, C. Li, Z. Xie, X. Jing, Ionic covalent-organic framework nanozyme as effective cascade catalyst against bacterial wound infection, Small 17 (2021) 2100756, https://doi.org/10.1002/smll.202100756.
[15] X. Cheng, S. Zhang, H. Liu, H. Chen, J. Zhou, Z. Chen, X. Zhou, Z. Xie, Q. Kuang, L. Zheng, Biomimetic metal-organic framework composite-mediated cascade catalysis for synergistic bacteria killing, ACS Appl. Mater. Interfaces 12 (2020) 36996–37005, https://doi.org/10.1021/acsami.0c12159.
[16] P. Wang, L. Peng, J. Lin, Y. Li, Q. Luo, S. Jiang, H. Tian, Y. Zhang, X. Liu, J. Liu, Enzyme hybrid virus-like hollow mesoporous CuO adhesive hydrogel spray through glucose-activated cascade reaction to efficiently promote diabetic wound healing, Chem. Eng. J. 415 (2021) 128901, https://doi.org/10.1016/j.cej.2021.128901.
[17] Z. Yu, W. Pan, N. Li, B. Tang, A nuclear targeted dual-photosensitizer for drug-resistant cancer therapy with NIR activated multiple ROS, Chem. Sci. 7 (2016) 4237–4244, https://doi.org/10.1039/C6SC 00737F.
[18] L. Pan, J. Liu, J. Shi, Intranuclear photosensitizer delivery and photosensitization for enhanced photodynamic therapy with ultralow irradiance, Adv. Funct. Mater. 24 (2014) 7318–7327, https://doi.org/10.1002/adfm.201402255.
[19] G. Subbiahdoss, S. Sharifi, D.W. Grijpma, S. Laurent, H.C. van der Mei, M. Mahmoudi, H.J. Busscher, Magnetic targeting of surface-modified superparamagnetic iron oxide nanoparticles yields antibacterial efficacy against biofilms of gentamicin-resistant staphylococci, Acta Biomater. 8 (2012) 2047–2055, https://doi.org/10.1016/j.actbio.2012.03.002.
[20] K. Quan, Z. Zhang, Y. Ren, H.J. Busscher, H.C. van der Mei, B.W. Peterson, Homogeneous distribution of magnetic, antimicrobial-carrying nanoparticles through an infectious biofilm enhances biofilm-killing efficacy, ACS Biomater. Sci. Eng. 6 (2019) 205–212, https://doi.org/10.1021/acsbiomate rials.9b01425.
[21] A. Elbourne, S. Cheeseman, P. Atkin, N.P. Truong, N. Syed, A. Zavabeti, M. Mohiuddin, D. Esrafilzadeh, D. Cozzolino, C.F. McConville, M.D. Dickey, R. J. Crawford, K. Kalantar-Zadeh, J. Chapman, T. Daeneke, V.K. Truong, Antibacterial liquid metals: biofilm treatment via magnetic activation, ACS Nano 14 (2020) 802–817, https://doi.org/10.1021/acsnano.9b07861.
[22] D.D. Thomas, X. Liu, S.P. Kantrow, J.R. Lancaster Jr., The biological lifetime of nitric oxide: implications for the perivascular dynamics of NO and O_2, Proc. Natl. Acad. Sci. Unit. States Am. 98 (2001) 355–360. https://www.jstor.org/stable/3054679.
[23] L. Ritsma, E.J. Steller, S.I. Ellenbroek, O. Kranenburg, I.H.B. Rinkes, J. van Rheenen, Surgical implantation of an abdominal imaging window for intravital microscopy, Nat. Protoc. 8 (2013) 583–594. http://www.nature.com/doifinder/10.1038/nprot.2013.026.
[24] M. Güemes, S.A. Rahman, K. Hussain, What is a normal blood glucose? Arch. Dis. Child. 101 (2016) 569–574, https://doi.org/10.1136/archdischild-2015-308336.
[25] H. Wei, E. Wang, Nanomaterials with enzyme-like characteristics (nanozymes): next-generation artificial enzymes, Chem. Soc. Rev. 42 (2013) 6060–6093, https://doi.org/10.1002/chin.201338273.
[26] T. Bjarnsholt, M. Alhede, M. Alhede, S.R. Eickhardt-Sørensen, C. Moser, M. Kühl, P. Ø. Jensen, N. Høiby, The *in vivo* biofilm, Trends Microbiol. 21 (2013) 466–474, https://doi.org/10.1016/j.tim.2013.0 6.002.
[27] Q. Zhang, Y. Liu, K.C. Chen, G. Zhang, X. Shi, H. Chen, Surface biocompatible modification of polyurethane by entrapment of a macromolecular modifier, Colloids Surf., B 102 (2013) 354–360, https://doi.org/10.1016/j.colsurfb.2012.07.037.
[28] G. Subbiahdoss, R. Kuijer, H.J. Busscher, H.C. van der Mei, Mammalian cell growth versus biofilm formation on biomaterial surfaces in an *in vitro* post-operative contamination model, Microbiology 156 (2010) 3073–3078, https://doi.org/10.1099/mic.0.040378-0.
[29] R. Wu, Y. Chong, G. Fang, X. Jiang, Y. Pan, C. Chen, J. Yin, C. Ge, Synthesis of Pt hollow nanodendrites with enhanced peroxidase-like activity against bacterial infections: implication for wound healing, Adv. Funct. Mater. 28 (2018) 1801484, https://doi.org/10.1002/adfm.201801484.
[30] W. Yin, J. Yu, F. Lv, L. Yan, L. Zheng, Z. Gu, Y. Zhao, Functionalized nano-MoS_2 with peroxidase catalytic and near-infrared photothermal activities for safe and synergetic wound antibacterial applications, ACS Nano 10 (2016) 11000–11011, https://doi.org/10.1021/acsnano.6b05810.
[31] L. Gao, K.M. Giglio, J.L. Nelson, H. Sondermann, A.J. Travis, Ferromagnetic nanoparticles with peroxidase-like activity enhance the cleavage of biological macromolecules for biofilm elimination, Nanoscale 6 (2014) 2588–2593, https://doi.org/10.1039/C3NR05422E.
[32] M.A. Islam, Einstein-Smoluchowski diffusion equation: a discussion, Phys. Scripta 70 (2004) 120. http://iopscience.iop.org/1402-4896/70/2-3/008.
[33] R. Roots, S. Okada, Estimation of life times and diffusion distances of radicals involved in X-ray-induced DNA strand breaks or killing of mammalian cells, Radiat. Res. 64 (1975) 306–320, https://doi.org/10.2307/3574267.
[34] D.M. Wood, A.L. Brennan, B.J. Philips, E.H. Baker, Effect of hyperglycaemia on glucose concentration of human nasal secretions, Clin. Sci. 106 (2004) 527–533, https://doi.org/10.1042/CS20030333.
[35] S. Tian, L. Su, Y. Liu, J. Cao, G. Yang, Y. Ren, F. Huang, J. Liu, Y. An, H.C. van der Mei, H.J. Busscher, L. Shi, Self-targeting, zwitterionic micellar dispersants enhance antibiotic killing of infectious biofilms-An intravital imaging study in mice, Sci. Adv. 6 (2020) eabb1112, http://advances.sciencemag.org/.
[36] D. Wang, G. Yang, H.C. van der Mei, Y. Ren, H.J. Busscher, L. Shi, Liposomes with water as a pH-responsive functionality for targeting of acidic tumor and infection sites, Angew. Chem. 60 (2021) 17714–17719, https://doi.org/10.1002/anie.202106329.
[37] K. Quan, G. Jiang, J. Liu, Z. Zhang, Y. Ren, H.J. Busscher, H.C. van der Mei, B. W. Peterson, Influence of interaction between surface-modified magnetic nanoparticles with infectious biofilm components in artificial channel digging and biofilm eradication by antibiotics *in vitro* and *in vivo*, Nanoscale 13 (2021) 4644–4653, https://doi.org/10.1039/D0NR08537E.
[38] F. Ullrich, C. Bergeles, J. Pokki, O. Ergeneman, S. Erni, G. Chatzipirpiridis, S. Pané, C. Framme, B.J. Nelson, Mobility experiments with microrobots for minimally invasive intraocular surgery, Invest. Ophthalmol. Vis. Sci. 54 (2013) 2853–2863, https://doi.org/10.1167/iovs.13-11825.